Interaction of charged impurities and Rydberg excitons in cuprous oxide

Sjard Ole Krüger,* Heinrich Stolz, and Stefan Scheel
Institut für Physik, Universität Rostock, Albert-Einstein-Straße 23-24, D-18059 Rostock, Germany

(Received 19 March 2020; revised manuscript received 11 May 2020; accepted 3 June 2020; published 16 June 2020)

We investigate the influence of a static, uncorrelated distribution of charged impurities on the spectrum of bound excitons in the copper oxide Cu_2O. We show that the statistical distribution of Stark shifts and ionization rates leads to the vanishing of Rydberg resonances into an apparent continuum. The appearance of additional absorption lines due to the broken rotational symmetry, together with spatially inhomogeneous Stark shifts, leads to a modification of the observed line shapes that agrees qualitatively with the changes observed in the experiment.

DOI: 10.1103/PhysRevB.101.235204

I. INTRODUCTION

Semiconductor Wannier excitons are quasiparticles comprising an electron and a hole bound by their mutual Coulomb interaction [1]. These states have first been observed in the 1950s in Cu_2O [2,3], where they appear as a series of resonances below the band gap and show remarkable resemblance to the hydrogenic Rydberg series. Recently, excitons with large principal quantum numbers of up to $n = 25$, termed Rydberg excitons, have been observed in Cu_2O [4]. These Rydberg excitons are very sensitive to perturbations of their surroundings, just as their atomic counterparts. For example, an intensity-dependent bleaching of the resonances has been observed [4], which has been interpreted as an excitonic Rydberg blockade. Furthermore, the deviations of the spectrum of Rydberg excitons from a purely hydrogenic series can be combined into a (phenomenological) quantum defect $\delta_{n,\ell}$ that is induced by the nonparabolic hole dispersion and other central-cell corrections [5–7].

Since their first observation, the influence of electric and magnetic fields on Rydberg excitons [8–12], the mutual dipole-dipole interaction between them [13], their fluorescence [14], and interexcitonic transitions [15] have been studied. Additionally, proposals have been put forward to use them for the implementation of masers [16,17] as well as the realization of topological spin phases in lattice potentials [18].

Another effect that has sparked substantial interest is the perturbation by free carriers, i.e., the electron-hole plasma [19,20]. It has been observed that the introduction of an electron-hole plasma by pumping above the band gap leads to a Mott transition for the Rydberg excitons. There, the band gap is lowered but the positions of the excitonic resonances are almost unaffected until the band gap crosses them, and the resonances vanish into the ionization continuum [19]. The apparent suppression of the highest exciton resonances follows a similar phenomenology as the Rydberg blockade mechanism. In addition to this plasma-induced shift of the band gap, the experiments revealed a static shift that is already present without the introduction of free charge carriers.

It has long been proposed that disorder introduced, e.g., by charged impurities might lead to the appearance of an exponential decay of the absorption coefficient below the band gap, as well as a shifted band gap [21]. Charged impurities may form in a compensated semiconductor, containing both acceptors and donors, as it can be energetically favorable for donor-acceptor pairs to ionize if their binding energies are sufficiently low, $E_A + E_D < E_g$ (see Sec. 7.1.3 in Ref. [22]). The main point defects present in a typical Cu_2O crystal are Cu and O vacancies [23,24] fulfilling this condition and acting as acceptors and donors, respectively. Depending on the density of these defects, however, the oxygen vacancies may form stable charged compound defects W^+ with copper vacancies [23,25] deep inside the band gap. In order for charge neutrality to be upheld, they would have to be compensated by an excess of charged copper vacancies V_{Cu}^- or free electrons. These charged impurities introduce a static electric field in which the exciton resonances may shift or ionize. This can result in a downward shift of the edge of the absorption continuum which can be interpreted as a reduction of the band gap. The influence of the static charged impurities can, at least for low densities of the impurities, be modeled by methods originally derived for atomic systems in ionic plasmas, the microfield distributions. These describe the statistical distribution of local electric fields which in turn induce statistically distributed Stark shifts and ionization broadening for the excitonic states. In the absence of a screening plasma, the suitable microfield distribution is the one derived by Holtsmark in 1919 [26] as all assumptions [static, uncorrelated, and (locally) homogeneous charge distribution] should be fulfilled. We will therefore use it in this work to assess the influence of charged impurities on the absorption spectra of the Rydberg excitons in Cu_2O.

The article is structured as follows: In Sec. II, we describe the modeling Hamiltonian used as well as the Holtsmark microfield distribution and discuss the central assumptions. In Sec. III, we will present the numerical spectra, analyze their line parameters, and compare them to experimental spectra.

*sjard.krueger@uni-rostock.de

Finally, we will provide a discussion of our results and an outlook in Sec. IV.

II. THEORY OF STARK-SHIFTED EXCITONS

The real-space Wannier equation for an exciton perturbed by external, static charges has the form

$$\left[\mathcal{H}_0 + \frac{e^2}{4\pi\varepsilon}\sum_i s_i\left\{\frac{1}{|\boldsymbol{r}_e-\boldsymbol{R}_i|}-\frac{1}{|\boldsymbol{r}_h-\boldsymbol{R}_i|}\right\}\right]\phi(\boldsymbol{r}_e,\boldsymbol{r}_h) = E\,\phi(\boldsymbol{r}_e,\boldsymbol{r}_h), \tag{1}$$

where $\mathcal{H}_0$ is the unperturbed excitonic Hamiltonian, $s_i = \pm 1$ is the sign of the perturbing charge, and $\varepsilon = \varepsilon_0\varepsilon_r$ is the crystal permittivity with $\varepsilon_r = 7.5$ [27]. Furthermore, $\boldsymbol{r}_{e/h}$ denote the coordinates of the electron and hole that form the exciton, and the $\boldsymbol{R}_i$ are the coordinates of the charged impurities. Focusing on only one of the charges, introducing center-of-mass and relative coordinates $\boldsymbol{R}$ and $\boldsymbol{r}$, respectively, as well as $\boldsymbol{\varrho}_i = \boldsymbol{R} - \boldsymbol{R}_i$, gives, for the interaction Hamiltonian $\mathcal{H}_i$,

$$\mathcal{H}_i = \frac{e^2}{4\pi\varepsilon}s_i\left\{\frac{1}{|\boldsymbol{\varrho}_i-\alpha\boldsymbol{r}|}-\frac{1}{|\boldsymbol{\varrho}_i+\beta\boldsymbol{r}|}\right\}, \tag{2}$$

where $\alpha = m_e/(m_e+m_h)$ and $\beta = m_h/(m_e+m_h)$ are the relative electron and hole masses, respectively. A Taylor expansion around $\boldsymbol{r} = \boldsymbol{0}$ up to first order in $\boldsymbol{r}$ yields

$$\mathcal{H}_i \approx \frac{e^2}{4\pi\varepsilon}s_i\frac{\boldsymbol{\varrho}_i\cdot\boldsymbol{r}}{|\boldsymbol{\varrho}_i|^3}, \tag{3}$$

and thus

$$\left[\mathcal{H}_0 + \frac{e^2}{4\pi\varepsilon}\sum_i s_i\frac{\boldsymbol{\varrho}_i\cdot\boldsymbol{r}}{|\boldsymbol{\varrho}_i|^3}\right]\phi(\boldsymbol{r}) = [\mathcal{H}_0 + e\boldsymbol{F}\cdot\boldsymbol{r}]\phi(\boldsymbol{r}) = E\,\phi(\boldsymbol{r}), \tag{4}$$

where

$$\boldsymbol{F} = \sum_i \boldsymbol{F}_i = \frac{e}{4\pi\varepsilon}\sum_i s_i\frac{\boldsymbol{\varrho}_i}{|\boldsymbol{\varrho}_i|^3} \tag{5}$$

is the total electric field of all charged impurities. Here, the implicit assumption has been made that the length scale on which $\boldsymbol{F}$ varies is large compared to the extension of excitonic states. In this case, the center-of-mass and relative coordinates can be separated if $\mathcal{H}_0$ also permits such a separation, and the truncation of the Taylor expansion after the first nonvanishing term is justified. We have tested this assumption via a Monte Carlo ansatz, implying that within the range of interest (defined by the radius of the largest observable excitons), the median relative deviation from the linear approximation is $<10\%$.

Under the assumption of a static, uncorrelated, and homogeneous distribution of perturbing charges, the microfield distribution can be derived from Eq. (5), yielding the Holtsmark distribution [26,28,29]

$$P(\xi)d\xi = \frac{2}{\pi}\xi\,d\xi\int_0^\infty dx\,x\,e^{-x^{3/2}}\sin(\xi\,x) \tag{6}$$

of the normalized electric field $\xi = |\boldsymbol{F}|/F_0$. The normalization factor F_0 corresponds closely to the field induced by a single impurity at a distance of $R_0 = \sqrt[3]{3/(4\pi\rho_{ci})}$,

$$F_0 = \frac{e}{2\varepsilon}\left[\frac{4\rho_{ci}}{15}\right]^{2/3} = \frac{e}{4\pi\varepsilon R_0^2}\left(\frac{8\pi}{25}\right)^{1/3} \approx \frac{e}{4\pi\varepsilon R_0^2}, \tag{7}$$

where ρ_{ci} denotes the density of charged impurities. R_0 coincides roughly with the average distance of the nearest-neighbor impurity at any point. The signs of the perturbing charges s_i are irrelevant, as long as the Taylor expansion in Eq. (3) is limited to the term linear in $\boldsymbol{r}$. Microfield distributions for more involved scenarios have been derived including, e.g., a screening plasma and charge-carrier correlations [30,31].

We will focus on the simplest scenario of unscreened charges interacting with hydrogenlike excitons fulfilling the nonparabolic Wannier equation

$$\mathcal{H}_0\,\phi(\boldsymbol{r}) = \left[\frac{\boldsymbol{p}^2}{2\mu} + \Delta T_h(\boldsymbol{p}^2) - \frac{e^2}{4\pi\varepsilon\,r}\right]\phi(\boldsymbol{r}) = E\,\phi(\boldsymbol{r}), \tag{8}$$

where $\Delta T_h(\boldsymbol{p}^2)$ is the nonparabolic part of the hole dispersion which is responsible for the excitonic quantum defects. The approach to solve this equation based on reformulating it as a Sturmian Coulomb problem [32] has been outlined in Ref. [5]. The relative absorption coefficients of the Stark spectra $\alpha_0(\omega,\boldsymbol{F})$ are then derived by diagonalization of the Wannier equation (4) in the basis of the eigenstates of $\mathcal{H}_0$.

If the Hamiltonian of the unperturbed exciton has $O(3)$ symmetry as in our model, the quantization axis can be chosen parallel to $\boldsymbol{F}$. In this case, the excitonic quantization axes are distributed statistically, which can be taken into account by regarding the exciting light field as unpolarized with respect to the quantization axis, which leads to spectra independent of the field direction $\alpha_0(\omega,\boldsymbol{F}) = \alpha_0(\omega,F) = A\,\hbar\omega\sum_i L_i(\omega,F)$ with some constant A.

The resonance line shapes are modeled by asymmetric Lorentzians [33]

$$L_i(\omega,F) = \frac{f_i}{\pi}\frac{\frac{\Gamma_i}{2} + 2q_i\,g\left(\frac{\omega-\omega_i}{\Gamma_i/2}\right)(\omega-\omega_i)}{(\omega-\omega_i)^2 + \left(\frac{\Gamma_i}{2}\right)^2}, \tag{9}$$

where f_i is the oscillator strength, Γ_i the full width at half maximum (FWHM) linewidth, ω_i the frequency, and q_i the asymmetry parameter of the ith resonance. For isolated P excitons, the asymmetry can be linked to the frequency dependence of the phononic scattering [33]. In the following, however, the q_i have to be interpreted as empirical parameters used to describe and compare the shapes of the absorption lines in the experimental and numerical spectra as the apparent change in the asymmetry is induced by the superposition of multiple lines. In our model, all of these parameters except for the q_i depend on the electric field F. The function $g(x)$ has been chosen as

$$g(x) = \begin{cases} 1 & \text{if } |x| \leqslant 4, \\ e^{-\left(\frac{|x|-4}{4}\right)^2} & \text{else.} \end{cases} \tag{10}$$

The corresponding line shape resembles an asymmetric Lorentzian with a constant asymmetry parameter in the vicinity of the resonance, and a symmetric Lorentzian far away from it. This line shape has been chosen as the use of asymmetric Lorentzians with constant asymmetry $g(x) = 1$ leads

TABLE I. Input FWHM linewidths in μeV taken from Ref. [35].

n	P	F	n	P	F
2	1896		3	648.4	
4	268.5	8.162	5	139.8	7.489
6	81.68	5.024	7	51.74	3.75
8	34.79	2.974	9	24.5	2.369
10	17.89	1.89	11	13.46	1.516
12	10.38	1.226	13	8.17	1.001
14	6.545	0.825	15	5.325	0.687
16	4.389	0.577	17	3.66	0.488
18	3.084	0.416	19	2.623	0.358
20	2.249	0.31	21	1.943	0.27
22	1.691	0.236	23	1.48	0.208
24	1.303	0.184			

to a linearly decreasing absorption at the band gap due to the long-range decay $\propto -(\omega-\omega_i)^{-1}$ of all resonances below it. This behavior is not observed in the experiment, where the absorption increases linearly at the band gap as predicted by Elliot [34] and reproduced by symmetric Lorentzians with their long-range decay $\propto(\omega-\omega_i)^{-2}$. With this choice of $g(x)$, the transition between the asymmetric and symmetric Lorentzian happens at about $2\Gamma_i$. The choice of the parameter 4 is somewhat arbitrary but the resulting spectra are not very sensitive to its exact choice.

The optical transition matrix elements $o_{n,\ell,m}$ from the crystal vacuum to the eigenstates of $\mathcal{H}_0$ are proportional to [34]

$$o_{n,\ell,m} \propto \begin{cases} \frac{\partial}{\partial r} R_{n\ell}(r)\big|_{r=0} & \text{if } \ell = 1, \\ 0 & \text{else}, \end{cases} \tag{11}$$

for unpolarized light, where $R_{n,\ell}(r)$ denotes the radial part of the real-space envelope function. The relative oscillator strengths of the Stark excitons can then be calculated via

$$f_i \propto |\boldsymbol{c}_i \cdot \boldsymbol{o}|^2, \tag{12}$$

where $\boldsymbol{c}_i$ is the ith algebraic eigenvector of the Hamiltonian in Eq. (4) and $\boldsymbol{o}$ is the vector of the relative transition matrix elements in Eq. (11), expressed in the chosen basis. The oscillator strengths of the unperturbed P excitons scale as $f_n \propto (n^2-1)/n^5$ due to the second-class nature of the transition from the crystal vacuum to the excitonic state [34] (i.e., the transition between the pure Bloch states of the valence and conduction band is dipole forbidden at the zone center due to parity).

The linewidths were calculated as laid out in Ref. [35] for the unperturbed P and F excitons[1] (see Table I). They contain all relevant phononic scattering paths into the yellow $1S$ and $2S$ excitons, namely, the scattering by longitudinal optic (LO) phonons via the Fröhlich mechanism and the deformation potential scattering by the $\Gamma_{3/5}^-$ phonons. For the S and D excitons, the experimental linewidths are not well described by this theory. We did therefore use extrapolated experimental results from second-harmonic generation (SHG) spectra [36] for the $3S$ and $3D$ state, respectively, giving $\Gamma_{nS} = 2\,\text{meV}\,n^{-3}$ and $\Gamma_{nD} = 3\,\text{meV}\,n^{-3}$. In addition, the complete experimental spectra seem to be broadened by 5–6 μeV. Figure 1 shows the experimental linewidths of one particular absorption spectrum. The deviation from the theoretically expected scaling $\propto(n^2-1)/n^5$ already observed in Ref. [4] could be explained by the convolution of the spectrum with a broadening Lorentzian, whose origin is unknown to us. We modeled it by adding 5.55 μeV to all input linewidths.

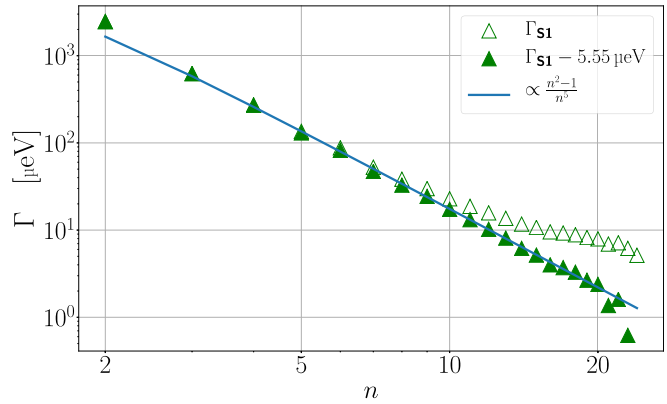

FIG. 1. Comparison of the linewidths derived from spectrum **S1** with the theoretically expected scaling (see Sec. III for details about the experimental spectra). The deviation can be explained by an additional broadening of 5.55 μeV for all lines.

The asymmetry of the lines was taken to be $q_i = -0.24$ for all lines, derived from fits to experimental spectra. Clearly, the model Hamiltonian in Eq. (4) evaluated in a basis of bound excitonic states can only be a reasonable description for Stark excitons that are themselves bound. This problem could be addressed by complex scaling techniques [11] or the introduction of a complex absorbing potential [37]. Fortunately, the states above the classical ionization threshold [38]

$$E_{\text{ion}}(F) = -\sqrt{\frac{e^3 F}{\pi\varepsilon}} \tag{13}$$

tend to be broadened by the ionization as well as the averaging over the microfield distribution as they are very sensitive to variations of the electric field. Our assumption is thus that the ionized states only contribute to a continuous background to the absorption spectrum but do not account for prominent absorption lines. Once the Stark spectra are calculated, the Holtsmark spectra can be derived via

$$\alpha(\omega,\rho_{ci}) = \frac{1}{F_0(\rho_{ci})}\int_0^\infty dF\, P\!\left(\frac{F}{F_0(\rho_{ci})}\right)\alpha_0(\omega,F). \tag{14}$$

The integration was performed on a logarithmic grid in F with $F_n/F_{n-1} = 1.001$ for field strengths from $1\,\text{mVm}^{-1}$ to $100\,\text{kVm}^{-1}$ via the finite difference summation $\int dF\, f(F) \approx \sum_n \Delta F_n\, f(F_n)$ where $\Delta F_n = (F_{n+1} - F_{n-1})/2$.

[1]Here and in the following, $\{S, P, D, F\}$ refers to states with the orbital quantum numbers $\ell = \{0, 1, 2, 3\}$, respectively, as is common in atomic physics. In general, ℓ is only a good quantum number if the Hamiltonian is invariant under the full rotation group SO(3), which cannot be the case in a solid state environment. In the cubic symmetry of Cu_2O, however, a spherically symmetric approximation is sufficiently good [5], as reflected by our choice of $\mathcal{H}_0$.

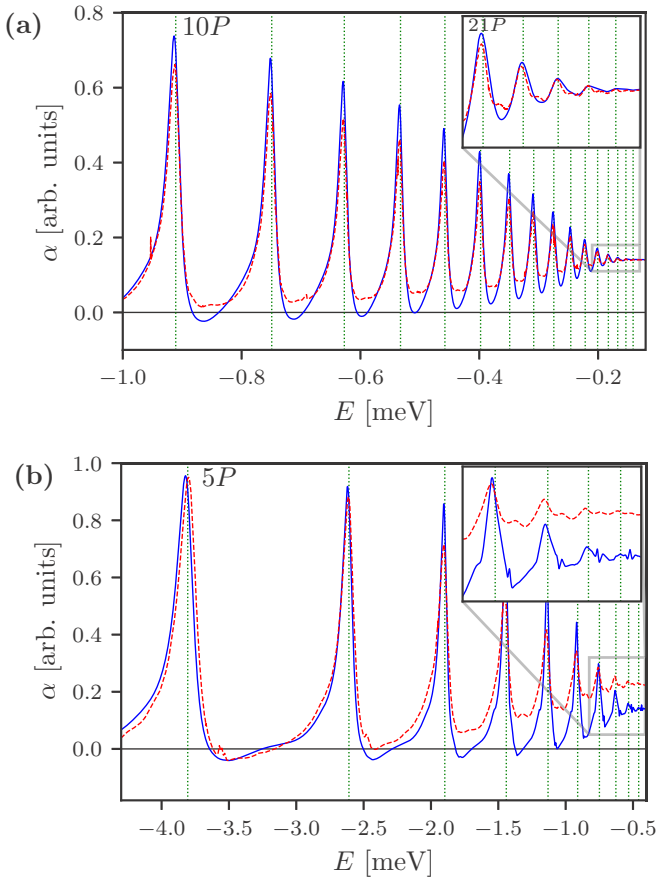

FIG. 2. Comparison of experimental spectra (dashed red lines) and numerical spectra (solid blue lines). (a) Comparison of spectrum **S1** to the numerical spectrum for $\rho_{ci} = 1.2 \times 10^9\,\mathrm{cm}^{-3}$. (b) **S2** vs numerical spectrum for $\rho_{ci} = 10^{11}\,\mathrm{cm}^{-3}$. The vertical lines represent the (numerical) positions of the unperturbed P excitons.

To summarize this section, the central assumptions of our model are as follows: (1) The charged impurities are static and their distribution is homogeneous and uncorrelated. (2) The electric field induced by the impurities varies on length scales considerably larger than the extension of the excitonic states of interest. (3) The spectral structure is dominated by bound excitons below the classical ionization threshold.

III. NUMERICAL RESULTS AND COMPARISON TO EXPERIMENTAL DATA

We will now apply our numerical method to the resonance spectrum of Rydberg excitons and compare with two experimental absorption spectra with maximum observable principal quantum numbers of $n_{\max} \approx 25$ (hereafter **S1**) and $n_{\max} \approx 13$ (hereafter **S2**). The spectrum **S1** measured at 1.2 K is the one used in the Ref. [4] and **S2** was measured at 1.3 K. The quantity $n_{\max}$ denotes the principal quantum number above which the resonances form an apparent absorption continuum and no individual lines can be resolved. There is, of course, some uncertainty in the definition of the highest observable principal quantum number $n_{\max}(\rho_{ci})$. In our analysis, a resonance was considered to have vanished as soon as its spectral range could not be reliably fitted with the line shape in Eq. (9).

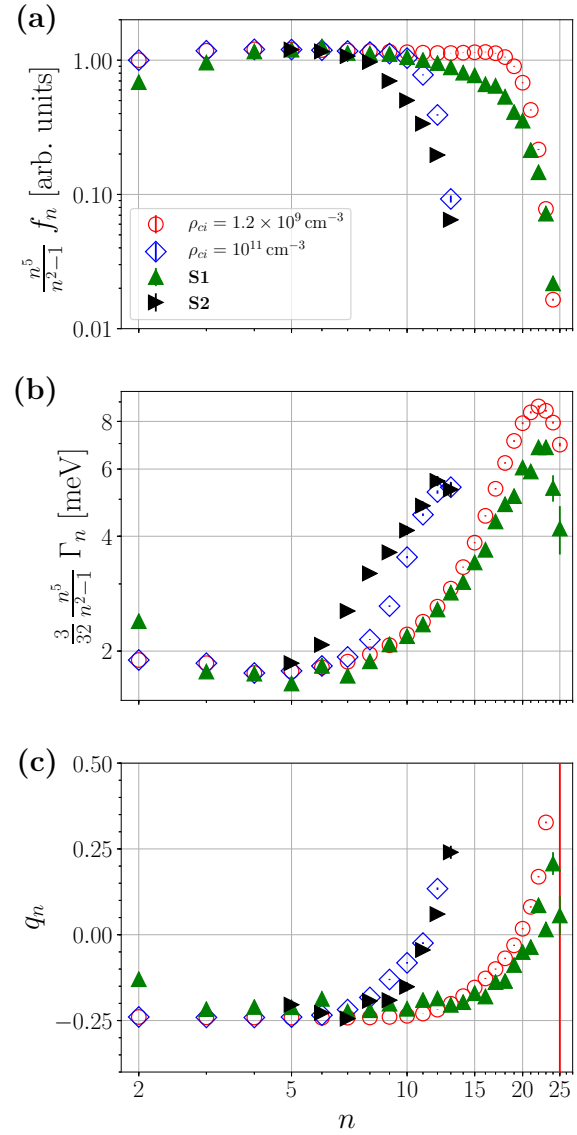

FIG. 3. The line parameters of Eq. (9) derived by fits to the numerical and experimental spectra for different impurity densities: (a) the oscillator strength, (b) the FWHM linewidths, and (c) the asymmetry parameter. The error bars denote one standard deviation.

Figure 2(a) compares **S1** with a numerical spectrum derived for $\rho_{ci} = 1.2 \times 10^9\,\mathrm{cm}^{-3}$ which was chosen to reproduce $n_{\max}$ while Fig. 2(b) compares **S2** to a numerical spectrum for $\rho_{ci} = 10^{11}\,\mathrm{cm}^{-3}$. The numerical spectrum in Fig. 2(b) shows weak additional lines corresponding predominantly to the S, D, and F excitons, which become dipole allowed due to the broken rotational symmetry (see inset). The original experimental spectra contain a background induced by the phonon-assisted absorption into the $1S$ and $2S$ states [39]. This background has been subtracted for the comparison with the numerical spectra, leading to the appearance of a negative absorption coefficient on the high-energy side of the lower resonances.

For the numerical computation, we took into account all states with $\ell \leqslant 25$, $n_r = n - \ell - 1 \leqslant 100$, as well as $m = 0, \pm 1$. This results in basis sets of dimension 2275 for $m = 0$ and 2175 for $m = \pm 1$. The calculation can be restricted to

these three magnetic quantum numbers as the Stark Hamiltonian has cylindrical symmetry which ensures that m remains a good quantum number (if the quantization axis is chosen as $z \parallel \boldsymbol{F}$) and the optically active P states can only be mixed into other states with $m = 0, \pm 1$.

One observes the following: (1) Excitons with large principal quantum numbers smear out and form an absorption continuum while the total oscillator strength is conserved. (2) The transition from negative asymmetry parameters q_n for low principal quantum numbers to positive ones for the highest n, which have been observed in experimental spectra, is reproduced. (3) Due to the breaking of the rotational symmetries by the Stark effect, additional absorption lines—corresponding to initially dark states—appear in the numerical spectra for high impurity densities. The strongest additional lines correspond to the S, D, and F states.

Figure 3 shows the line parameters derived by fits to the numerical spectra under the assumption that the underground below each line is constant over its width. The oscillator strength f [Fig. 3(a)] drops off steeply before the lines vanish starting at $n \approx 2n_{\max}(\rho_{ci})/3$, an observation that could be explained by neither plasma nor phonon interactions [20]. Compared to the experiment, however, the oscillator strength follows the $(n^2 - 1)/n^5$ scaling for longer and drops off more steeply for large n. Note that the experimental oscillator strengths in Fig. 3(a) have been normalized to the numerical ones at $n = 5$ as their absolute values cannot be compared.

The FWHM linewidths [Fig. 3(b)] start to deviate from the linewidths of the unperturbed resonances $n \approx n_{\max}(\rho_{ci})/2$ and drop off shortly before $n_{\max}(\rho_{ci})$. Additional inhomogeneous broadening could be introduced by an inhomogeneous straining of the crystal, the ionisation of states below the classical ionisation threshold [10] or the higher orders of the Taylor expansion, Eq. (3), which will become relevant when the electric field varies on the length scale of the exciton diameter. Furthermore, there could be additional sources of microfields with different microfield distributions, for example, optical phonons [21] or surface charges. The asymmetry parameter q [Fig. 3(c)] deviates from the value for the unperturbed lines for large principal quantum numbers and changes sign for $n \approx 4\, n_{\max}(\rho_{ci})/5$.

From the numerical spectra, we can extract the maximally observable principal quantum number as well as the shift of the band gap. Figure 4 shows the dependence of this band-gap shift on the density ρ_{ci} of charged impurities. To a good approximation, it follows a power law $\Delta E_g(\rho_{ci}) = -(0.71 \pm 0.17)\ \mu\text{eV}(\rho_{ci}/\text{cm}^{-3})^{0.254\pm0.011} \propto \rho_{ci}^{1/4}$. This scaling agrees with the dependence of the band-gap shift on the plasma density derived from many-body theory [20]. In our case, however, this is a purely empirical observation. We have not investigated whether this scaling holds outside the range of impurity densities given here. Clearly, it will have to break down at some point for large ρ_{ci}, as the assumptions made in the derivation of the Holtsmark distribution break down.

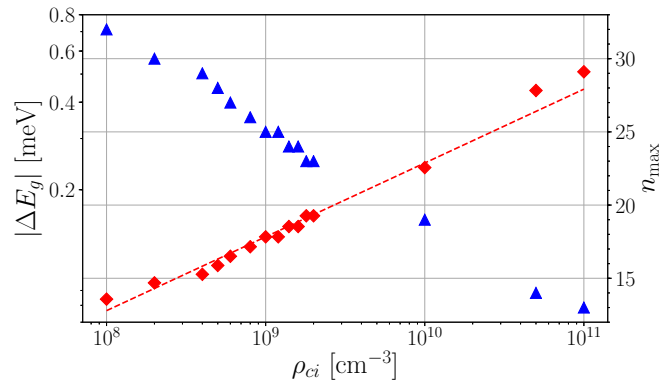

FIG. 4. The band-gap shift $\Delta E_g(\rho_{ci})$ (red diamonds) with a power-law fit (dashed line) and the maximum observable principal quantum number $n_{\max}(\rho_{ci})$ (blue triangles).

IV. DISCUSSION AND OUTLOOK

In this work, we have numerically investigated the influence of charged impurities on the spectrum of (Rydberg) excitons in Cu_2O. Our calculations reproduce experimentally observed phenomena such as the vanishing of the resonances with high principal quantum numbers into an apparent absorption continuum, accompanied by a drop of the oscillator strength of the discernible lines, a broadening as well as a change of the line shape towards positive asymmetry parameters q.

The breaking of the rotational symmetries inherent in our model leads to the redistribution of oscillator strength to initially dark states and the corresponding appearance of weak additional absorption lines in the spectra for impurity densities greater $\sim 10^{10}$ cm^{-3}. In the experimental spectrum **S2** [Fig. 2(b)] there are indeed some indications for such peaks, however, the signal-to-noise ratio of the present spectrum does not allow for a conclusive analysis. In every case, the nonappearance of such peaks may be used to establish an upper bound on the charged impurity density of given crystal samples.

ACKNOWLEDGMENTS

We thank Prof. M. Bayer and his group at the TU Dortmund for sharing their experimental data and D. Semkat (Greifswald) for helpful discussions. We acknowledge support by the Deutsche Forschungsgemeinschaft (DFG) within the SPP 1929 "Giant Interactions in Rydberg Systems (GiRyd)."

[1] G. H. Wannier, The structure of electronic excitation levels in insulating crystals, Phys. Rev. **52**, 191 (1937).

[2] E. F. Gross and N. A. Karryev, Opticheskii spektr eksitona, Dokl. Akad. Nauk SSSR **84**, 471 (1952).

[3] E. F. Gross, Optical spectrum of excitons in the crystal lattice, Nuovo Cimento **3**, 672 (1956).

[4] T. Kazimierczuk, D. Fröhlich, S. Scheel, H. Stolz, and M. Bayer, Giant Rydberg excitons in the copper oxide Cu_2O, Nature (London) **514**, 343 (2014).

[5] F. Schöne, S. O. Krüger, P. Grünwald, H. Stolz, S. Scheel, M. Aßmann, J. Heckötter, J. Thewes, D. Fröhlich, and M. Bayer, Deviations of the exciton level spectrum in Cu_2O from the hydrogen series, Phys. Rev. B **93**, 075203 (2016).

[6] F. Schweiner, J. Main, M. Feldmaier, G. Wunner, and C. Uihlein, Impact of the valence band structure of Cu_2O on excitonic spectra, Phys. Rev. B **93**, 195203 (2016).

[7] A. Alvermann and H. Fehske, Exciton mass and exciton spectrum in the cuprous oxide, J. Phys. B: At., Mol. Opt. Phys. **51**, 044001 (2018).

[8] F. Schweiner, J. Main, G. Wunner, M. Freitag, J. Heckötter, C. Uihlein, M. Aßmann, D. Fröhlich, and M. Bayer, Magnetoexcitons in cuprous oxide, Phys. Rev. B **95**, 035202 (2017).

[9] M. Kurz, P. Grünwald, and S. Scheel, Excitonic giant-dipole potentials in cuprous oxide, Phys. Rev. B **95**, 245205 (2017).

[10] J. Heckötter, M. Freitag, D. Fröhlich, M. Aßmann, M. Bayer, M. A. Semina, and M. M. Glazov, Dissociation of excitons in Cu_2O by an electric field, Phys. Rev. B **98**, 035150 (2018).

[11] P. Zielinski, P. Rommel, F. Schweiner, and J. Main, Rydberg excitons in electric and magnetic fields obtained with the complex-coordinate-rotation method, J. Phys. B: At., Mol. Opt. Phys. **53**, 054004 (2020).

[12] S. Artyukhin, D. Fishman, C. Faugeras, M. Potemski, A. Revcolevschi, M. Mostovoy, and P. H. van Loosdrecht, Magneto-absorption spectra of hydrogen-like yellow exciton series in cuprous oxide: Excitons in strong magnetic fields, Sci. Rep. **8**, 1 (2018).

[13] V. Walther, S. O. Krüger, S. Scheel, and T. Pohl, Interactions between Rydberg excitons in Cu_2O, Phys. Rev. B **98**, 165201 (2018).

[14] M. Takahata and N. Naka, Photoluminescence properties of the entire excitonic series in Cu_2O, Phys. Rev. B **98**, 195205 (2018).

[15] S. O. Krüger and S. Scheel, Interseries transitions between Rydberg excitons in Cu_2O, Phys. Rev. B **100**, 085201 (2019).

[16] D. Ziemkiewicz and S. Zielińska-Raczyńska, Proposal of tunable Rydberg exciton maser, Opt. Lett. **43**, 3742 (2018).

[17] D. Ziemkiewicz and S. Zielińska-Raczyńska, Solid-state pulsed microwave emitter based on Rydberg excitons, Opt. Exp. **27**, 16983 (2019).

[18] A. N. Poddubny and M. M. Glazov, Topological Spin Phases of Trapped Rydberg Excitons in Cu_2O, Phys. Rev. Lett. **123**, 126801 (2019).

[19] J. Heckötter, M. Freitag, D. Fröhlich, M. Aßmann, M. Bayer, P. Grünwald, F. Schöne, D. Semkat, H. Stolz, and S. Scheel, Rydberg Excitons in the Presence of an Ultralow-Density Electron-Hole Plasma, Phys. Rev. Lett. **121**, 097401 (2018).

[20] D. Semkat, H. Fehske, and H. Stolz, Influence of electron-hole plasma on Rydberg excitons in cuprous oxide, Phys. Rev. B **100**, 155204 (2019).

[21] J. D. Dow and D. Redfield, Toward a unified theory of Urbach's rule and exponential absorption edges, Phys. Rev. B **5**, 594 (1972).

[22] P. Yu and M. Cardona, *Fundamentals of Semiconductors: Physics and Materials Properties* (Springer, Berlin, 2010).

[23] F. Biccari, Defects and doping in Cu_2O, Ph.D. thesis, Universita di Roma, 2009.

[24] T. Ito and T. Masumi, Detailed examination of relaxation processes of excitons in photoluminescence spectra of Cu_2O, J. Phys. Soc. Jpn. **66**, 2185 (1997).

[25] M. Zouaghi, B. Prevot, C. Carabatos, and M. Sieskind, Near infrared optical and photoelectric properties of Cu_2O. III. Interpretation of experimental results, Phys. Status Solidi A **11**, 449 (1972).

[26] J. Holtsmark, Über die Verbreiterung von Spektrallinien, Ann. Phys. **363**, 577 (1919).

[27] C. Carabatos, A. Diffiné, and M. Sieskind, Contribution à l'étude des bandes fondamentales de vibration du réseau de la cuprite (Cu_2O), J. Phys. (Paris) **29**, 529 (1968).

[28] I. T. Iakubov, G. Kobzev, and M. Popovich, *Transport and Optical Properties of Nonideal Plasma* (Springer, Berlin, 2013).

[29] A. K. Pradhan and S. N. Nahar, *Atomic Astrophysics and Spectroscopy* (Cambridge University Press, Cambridge, UK, 2011).

[30] C. Hooper, Jr., Electric microfield distributions in plasmas, Phys. Rev **149**, 77 (1966).

[31] C. Hooper, Jr., Low-frequency component electric microfield distributions in plasmas, Phys. Rev. **165**, 215 (1968).

[32] R. Szmytkowski, Alternative approach to the solution of the momentum-space Schrödinger equation for bound states of the N-dimensional Coulomb problem, Ann. Phys. **524**, 345 (2012).

[33] Y. Toyozawa, Interband effect of lattice vibrations in the exciton absorption spectra, J. Phys. Chem. Solids **25**, 59 (1964).

[34] R. Elliott, Intensity of optical absorption by excitons, Phys. Rev. **108**, 1384 (1957).

[35] H. Stolz, F. Schöne, and D. Semkat, Interaction of Rydberg excitons in cuprous oxide with phonons and photons: Optical linewidth and polariton effect, New J. Phys. **20**, 023019 (2018).

[36] J. Mund, D. Fröhlich, D. R. Yakovlev, and M. Bayer, High-resolution second harmonic generation spectroscopy with femtosecond laser pulses on excitons in Cu_2O, Phys. Rev. B **98**, 085203 (2018).

[37] J. Grimmel, M. Stecker, M. Kaiser, F. Karlewski, L. Torralbo-Campo, A. Günther, and J. Fortágh, Ionization spectra of highly Stark-shifted rubidium Rydberg states, Phys. Rev. A **96**, 013427 (2017).

[38] T. F. Gallagher, *Rydberg Atoms*, Vol. 3 (Cambridge University Press, Cambridge, UK, 2005).

[39] F. Schöne, H. Stolz, and N. Naka, Phonon-assisted absorption of excitons in Cu_2O, Phys. Rev. B **96**, 115207 (2017).